

Vacancy Formation and Oxidation Characteristics of Single Layer TiS_3

F. Iyikanat,^{1,*} H. Sahin,^{2,†} R. T. Senger,¹ and F. M. Peeters²

¹*Department of Physics, Izmir Institute of Technology, 35430 Izmir, Turkey*

²*Department of Physics, University of Antwerp,
Groenenborgerlaan 171, B-2020 Antwerpen, Belgium*

(Dated: May 23, 2021)

Abstract

The structural, electronic and magnetic properties of pristine, defective and oxidized monolayer TiS_3 are investigated using first-principles calculations in the framework of density functional theory. We found that a single layer of TiS_3 is a direct band gap semiconductor and the bonding nature of the crystal is fundamentally different from other transition metal chalcogenides. The negatively charged surfaces of single layer TiS_3 makes this crystal a promising material for lubrication applications. The formation energies of possible vacancies, i.e. S, Ti, TiS and double S, are investigated via total energy optimization calculations. We found that the formation of a single S vacancy was the most likely one among the considered vacancy types. While a single S vacancy results in a nonmagnetic, semiconducting character with an enhanced band gap, other vacancy types induce metallic behavior with spin polarization of $0.3 - 0.8 \mu_B$. The reactivity of pristine and defective TiS_3 crystals against oxidation was investigated using conjugate gradient calculations where we considered the interaction with atomic O, O_2 and O_3 . While O_2 has the lowest binding energy with $0.05 - 0.07$ eV, O_3 forms strong bonds stable even at moderate temperatures. The strong interaction ($3.9 - 4.0$ eV) between atomic O and TiS_3 results in dissociative adsorption of some O-containing molecules. In addition, the presence of S-vacancies enhances the reactivity of the surface with atomic O whereas, it had a negative effect on the reactivity with O_2 and O_3 molecules.

PACS numbers: 73.20.Hb, 82.45.Mp, 73.61.-r, 73.90.+f, 68.55.Ln

I. INTRODUCTION

The wide range of different structural forms and the tunability of their electronic properties, has made two-dimensional ultra-thin materials popular in the field of condensed matter physics. In the last decade, following the synthesis of graphene,^{1,2} layered crystals of transition metal dichalcogenides (TMDs) have attracted tremendous interest owing to their remarkable electronic, mechanical and optical properties.³⁻⁵ Depending on the combination of metal and chalcogen atoms, TMDs may display metallic, semimetallic, semiconducting and even superconducting behavior.⁶⁻¹¹ Various experimental methods to thin down TMDs to monolayers¹²⁻¹⁴ and a number of theoretical studies revealing the possibility of tuning their properties have already been reported.¹⁵⁻¹⁸ In addition to TMDs (MoX_2 X= S, Se, Te) having graphene-like crystal structure, recent efforts have also led to the synthesis of novel TMDs with entirely different crystal structures. Titanium trisulphide (TiS_3) is one of the most recent examples of such layered transition metal chalcogenides.

The atomic structure belongs to the space group $\text{P}2_1/\text{m}$ and TiS_3 crystallizes in bundles of molecular chains that are formed by trigonal prisms, where the metal atoms occupy the centers of the prisms.^{19,20} Finkman *et al.*²¹ have shown that TiS_3 crystals are semiconducting with extrinsic n-type conductivity that have room temperature mobility of $30 \text{ cm}^2/(\text{V sec})$. Recently, strong nonlinearity of the current–voltage characteristics has been reported by Gorlava *et al.*^{22,23} In contrast to many other layered TMDs which exhibit an indirect to direct band gap transition at the monolayer limit, TiS_3 exhibits a direct band gap even for a width of hundreds of layers. Direct optical transitions with a band gap of 1.10 eV have been detected in thin films of TiS_3 .²⁴ Moreover, these thin films show photocurrent response to white light illumination.²⁵

Using high-resolution TEM for defective crystals, a metal-to-insulator transition with charge localization below $T_{MI} \approx 325 \text{ K}$ has been proposed by Guilmeau *et al.*²⁶ Their studies revealed that TiS_3 has low thermal conductivity and a large absolute value of the Seebeck coefficient at high temperatures. In a recent study by Island *et al.*²⁷ field effect transistors (NR-FET) have been fabricated at room temperature by isolating few-layer TiS_3 nanoribbons. The electron mobility of few-layer TiS_3 was found to be $2.6 \text{ cm}^2/(\text{V sec})$, and exhibits n-type semiconductor behavior with ultrahigh photoresponse and fast switching times. Furthermore, Island *et al.*²⁸ have isolated single-layer TiS_3 by mechanical exfoliation.

In this study, motivated by the latest experimental^{27–32} and theoretical^{33,34} studies on TiS₃, we investigated: (i) structural and electronic properties of single layer TiS₃, (ii) formation of vacancies in the pristine material and their influence on electronic properties, and (iii) environmental stability of its surface against oxidation. The paper is organized as follows. In Sec. II, we present the details of the computational methodology. Geometric, electronic and magnetic properties of defect-free TiS₃ and of various vacancy defects are given in Sec. III and Sec. IV, respectively. The response of pristine and defective TiS₃ to oxidation is analyzed in Sec. V. Results are discussed in Sec. VI.

II. COMPUTATIONAL METHODOLOGY

All the calculations were performed within the spin-polarized density functional theory (DFT) using projector-augmented-wave potentials (PAW) and a plane-wave basis set as implemented in the Vienna ab initio simulation package (VASP).^{35,36} The cutoff energy for the plane-waves was chosen to be 500 eV. Perdew-Burke-Ernzerhofs (PBE) version of generalized gradient approximation (GGA)³⁷ was used for the description of the exchange correlation functional. For a better approximation of bandgap values, underestimated by PBE functional, the HSE06 functional was also used.³⁸ In the HSE06 approach, the fraction of the Hartree-Fock exchange and the screening parameter were set to $\alpha = 0.25$ and 0.2 \AA^{-1} , respectively.

Spin-polarized calculations were performed in all cases and atomic charges were calculated using the Bader charge population analysis.³⁹ The Gaussian smearing method was employed for total energy calculations with a width of 0.01 eV. Density functional theory plus the long-range dispersion correction (DFT+D2) method was used to calculate the non-local correlation energies.⁴⁰ C_6 values of Ti and S atoms were 10.800 and 5.570, respectively. 1.562 and 1.683 were used as the vdW radius of Ti and S atoms, respectively.⁴⁰

Geometric structures of the perfect, vacancy defected and oxidized monolayer TiS₃ were fully optimized to minimize each component of the inter-atomic Hellmann-Feynman forces until a precision of 10^{-4} eV/\AA was reached. The pressure in the unit cell was kept below 1 kBar. The convergence criterion for energy was chosen to be 10^{-5} eV between two consecutive steps. The conjugate gradient method was used to compute lattice constants and total energies. In all cases, lattice parameters were optimized along the a_1 and a_2 directions. In

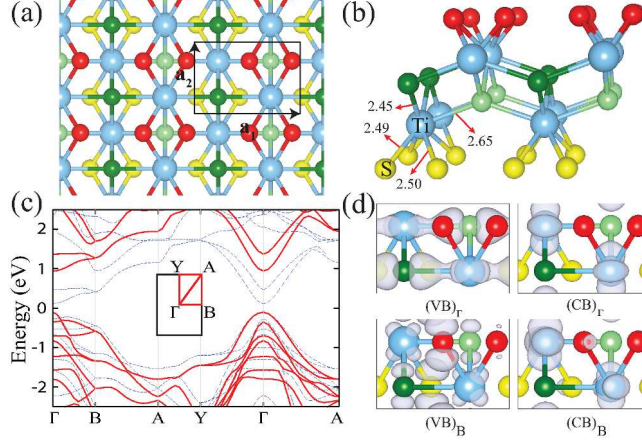


FIG. 1: (Color online) (a) Top view of monolayer TiS_3 and its unit cell shown by a rectangle. For a better top view, S atoms in different layers are presented by different colors. (b) Tilted side view of $2 \times 2 \times 1$ supercell of monolayer TiS_3 . (c) Blue dashed lines and red lines illustrate PBE and HSE06 results for the electronic band diagram of monolayer TiS_3 , respectively. (d) Band decomposed charge densities of valance band (VB) and conductance band (CB) at Γ and B.

order to hinder interlayer interaction within the periodic images, a vacuum spacing of 16 Å between adjacent layers was chosen. The lateral distance between vacancies (adsorbed atoms) was at least 10 Å in order to eliminate the interaction between vacancies (adsorbed atoms) in neighboring supercells. For the unitcell of TiS_3 , $19 \times 19 \times 1$ k-point mesh was used in PBE calculations, whereas due to high computational cost, the k-point mesh was reduced to $5 \times 5 \times 1$ in HSE calculations. For the supercell calculations, the same k-point mesh of $3 \times 3 \times 1$ was used for both PBE and HSE. The vacancies were obtained by removing the considered atoms from a 3×3 supercell which consist of 18 Ti atoms and 54 S atoms.

The calculated formation energies of the vacancies was obtained from $E_F = E_{M-A} - E_M + nE_A$, where E_F is the formation energy of the relevant vacancy, E_{M-A} is the total energy of the supercell with vacancy, n is the number of removed atoms, E_A is the energy of the removed atom and E_M is the energy of monolayer TiS_3 . Binding energies of O, O_2 and O_3 were calculated for the most favorable adsorption sites. These binding energies were calculated from the expression $E_B = E_{M+A}(E_{D+A}) - E_M(E_D) - mE_A$, where E_B is the binding energy of the adsorbed atom on pristine (S defected) TiS_3 , m is the number of adsorbed atoms, E_M (E_D) and E_{M+A} (E_{D+A}) are the total energy of pristine (S defected) and the adsorbed atom-pristine (adsorbed atom-S-defected) system, respectively.

III. PRISTINE SINGLE LAYER TiS_3

The unit cell of monolayer TiS_3 is a rectangular prism and is composed of 2 Ti atoms and 6 S atoms. The coordination of these atoms are illustrated by the top and tilted-side views in Figs. 1(a) and 1(b), respectively. The monolayer TiS_3 is composed of chain-like structures consisting of trigonal prisms with the metal atom occupying the centers of these prisms. In this phase, chains are parallel to the a_2 and they form layers in the $a_1 a_2$ plane, which are coupled with each other by the van der Waals interaction to form the bulk layered structure of TiS_3 . Our calculations show that monolayer TiS_3 has lattice vectors $a_1 = 4.99 \text{ \AA}$ and $a_2 = 3.39 \text{ \AA}$. These lattice parameters are comparable to the experimental bulk results $a_1 = 4.958 \text{ \AA}$, $a_2 = 3.4006 \text{ \AA}$, $a_3 = 8.778 \text{ \AA}$, and $\beta = 97.32$.^{19,20} As shown in Fig. 1(b) the bond distances of Ti atom and two different surface S atoms (red or yellow S atoms) are 2.49 \AA and 2.50 \AA , respectively. At the same time, these two surface S atoms are two of the three base S atoms of the trigonal prisms. The bond distance of Ti atom and third base S atom (dark or light green S atoms) of the trigonal prism is 2.45 \AA . The atom-atom distance of Ti atom and S atom (light or dark green S atoms) of neighboring prism is 2.65 \AA .

Charge density analysis is an efficient way to discuss the character of the interatomic interactions and bonding. In Fig. 2, we present a cross section of the 3D total charge density. Bader charge analysis shows that in parallel to their electronegativity values a significant amount of charge is transferred from Ti to the S atoms. While two S atoms at the surface (shown by red balls) share 0.7 electrons donated by the underlying Ti atom, 0.8 electron transfer occurs from Ti to S atom in the middle of the crystal (shown by light green balls). Thus, Ti-S bonds between surface and inner S atoms have an entirely different character. As is also delineated in Fig. 2 the bond between Ti and inner S atoms is constructed through 0.8 electron transfer and therefore it has an ionic character. However, the bonds between Ti and surface S atoms are constructed through relatively less electron transfer and hence it has mostly covalent character. It is also seen from Fig. 2 that each surface atom interacts with neighboring S atoms while there is no contact between the inner S atoms. Therefore one expects anisotropic electronic and transport properties due to the varying character of the surface states along a_1 and a_2 directions. It is also worth mentioning that the negatively charged surface of monolayer TiS_3 may find interesting applications such as nanoscale lubricants and charged coatings.

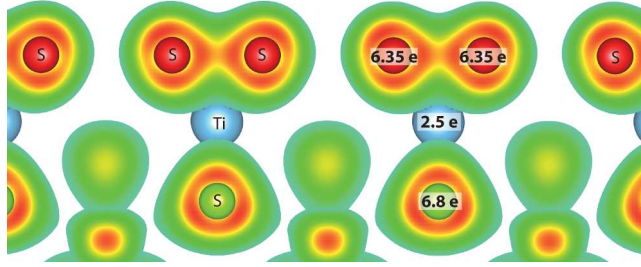


FIG. 2: (Color online) Cross-sectional plane view of the charge densities, with two surface, and one inner S atom placed at this plane. Valance charges on inner and outer S atoms are also shown. Color code of atoms is the same as in Fig. 1. Electron density increases from green to red.

Calculated band diagrams of pristine TiS_3 using PBE and HSE06 methods are shown in Fig. 1(c). It is known that often the values, obtained with the PBE functional underestimates the energy band gaps of semiconductors. The band gap of TiS_3 is calculated to be 0.23 eV by using the PBE approximation. However, including the HSE06 correction one gets a 1.05 eV direct band gap at the Γ point, which is in good agreement with the experimental value of 1.10 eV, for few-layer TiS_3 .^{24,25} For further analysis of the band structure of TiS_3 , charge densities of the valance band maximum (VB) and the conduction band minimum (CB) at the Γ and the B high-symmetry points are shown in Fig. 1(d). It is seen that the VB is composed of $2p_x$ orbitals of S and $3d_{xz}$ orbitals of Ti and they form a strong bond, whereas the main contribution to the CB edge comes from $3d_{y^2-z^2}$ orbitals of Ti atom at the Γ point. At the B point, p_y orbitals of S atoms dominant while $3d_{xy}$ orbitals of Ti atom contribute slightly to the VB. In particular, p orbitals of surface S atoms are larger than p orbitals of the inner S atoms. Thus, the main contribution to the VB is dominated by p_y orbitals of the surface S atoms. Like at the Γ point, while the S atoms do not contribute significantly, all the contribution comes from the $3d_{y^2-z^2}$ orbitals of the Ti atom to the CB. In the trigonal prisms every Ti atom shares 4 valence electrons with 3 base S atoms and 1 neighboring chain S atom. Due to the lack of any unsaturated orbitals, monolayer TiS_3 has a nonmagnetic ground state.

TABLE I: Lattice parameters, formation energies, magnetic moments, electronic characteristics and band gaps of 3×3 supercell of monolayer TiS_3 and its few defected forms calculated using PBE method. HSE06 results for the band gap of semiconductors are also given.

	a_1 / a_2 (Å)	E_F (eV)	m (μB)	Electronic Characteristic	Band Gap (eV)
Pristine TiS_3	14.98 / 10.18	-	0.0	Semiconductor	0.23(PBE)/1.05(HSE06)
S Vacancy	14.90 / 10.17	3.58	0.0	Semiconductor	0.28(PBE)/0.89(HSE06)
Ti Vacancy	15.05 / 10.14	12.00	0.5	Metal	-
Double S Vacancy	14.96 / 10.18	8.48	0.8	Metal	-
Ti, S Vacancy	14.90 / 10.13	16.15	0.3	Metal	-

IV. DEFECTIVE SINGLE LAYER TiS_3

A. S-vacancy

The first defective structure we consider is a single S vacancy in TiS_3 monolayer. To compare the geometric structure of monolayer TiS_3 in the presence and absence of a vacancy, a 3×3 supercell is considered and the lattice vectors for the defect-free TiS_3 computational supercell are found as $a_1 = 14.98 \text{ \AA}$ and $a_2 = 10.18 \text{ \AA}$. Fully relaxed geometric structure when a single S atom is removed from the surface of monolayer TiS_3 is shown in Fig. 3(a). When S vacancy is introduced the lattice vectors of 3×3 supercell change and become $a_1 = 14.90 \text{ \AA}$ and $a_2 = 10.17 \text{ \AA}$. Thus, the presence of the S vacancy leads to a minute shrinkage of the lattice vectors of TiS_3 . As can be seen from Fig. 3(a), the nearest surface S atom to the vacancy follows the direction of the arrow, localizes on top of the inner S atom (light green) and forms reconstructed bonds with the nearest Ti atoms with a bond length of 2.32 \AA . Bader charge analysis tells us that, the total charge of this atom is increased by 0.4 electrons when removing the nearest neighbor S atom. The charges of other atoms do not change significantly with the removal of the surface S atom. Our calculated results show that the formation energy of an S-vacancy is 3.58 eV.

To calculate the electronic properties of S-vacancy defected monolayer TiS_3 in addition to PBE, HSE06 method is also used and the results are listed in Table I. Moreover, the density of states (DOS) of pristine and S-atom-removed TiS_3 calculated by PBE method

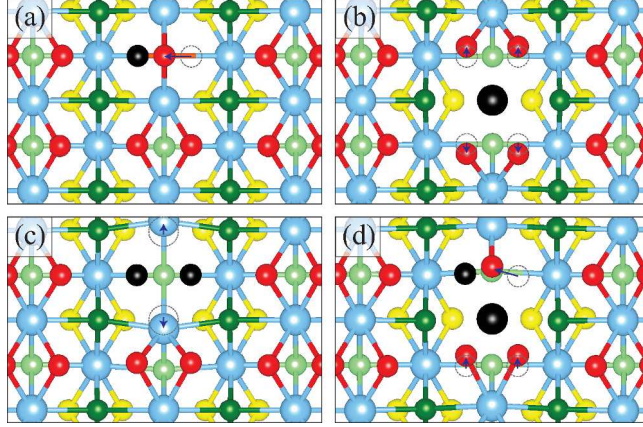


FIG. 3: (Color online) Top view of relaxed monolayer TiS_3 with (a) S-vacancy, (b) Ti-vacancy, (c) Double S-vacancy, (d) TiS-vacancy. Black atoms illustrate removed atoms, dashed circles show initial position of the displaced atom. Color code of the other atoms is the same as in Fig. 1. The direction of displaced atoms are depicted by blue arrows.

are shown in Figs. 4(a) and 4(b), respectively. As can be seen from the figures and Table I, removing one S atom from the surface of TiS_3 does not make any notable effect on the electronic structure of TiS_3 . The monolayer conserves its semiconductor character. Due to the reconstruction of the S atom and its binding with 2 Ti atoms, there are no unsaturated bonds. Thus, the nonmagnetic character of the TiS_3 is preserved during the formation of an S-vacancy.

B. Ti-vacancy

Relaxed geometric structure when a single Ti atom is extracted from TiS_3 is illustrated in Fig. 3(b). A significant surface reconstruction is observed after geometric relaxation. This figure shows that, when one Ti atom is taken out, the displacement of the inner S atoms that were attached to it, is not significant, nevertheless they lose 0.1 electrons. However, the four surface S atoms are released, they move towards the other Ti atoms and they lose approximately 0.2 electrons. This gives rise to an expansion in the lattice parameter a_1 , which after relaxation becomes $a_1 = 15.05 \text{ \AA}$ and $a_2 = 10.14 \text{ \AA}$. Hence, removal of Ti atom leads to an increase in a_1 , whereas a decrease in a_2 . The formation energy of Ti-vacancy is 12.00 eV. Defects with high formation energies are unlikely to form, and therefore an S-vacancy will have a much higher probability to form as compared to a Ti-vacancy.

Unlike S vacancy, Ti vacancy has a major effect on the electronic structure of TiS_3 , it loses its semiconductor character and becomes metallic. As shown in Fig 4(c) the states originating from Ti vacancy are near the VB with three peaks of gap states arising from the mixture of the orbitals of the neighboring S and Ti atoms. This leads the possibility of p-type doping if Ti vacancy can be created. As seen from Fig. 4(c), at the Fermi level, there is a slight spin polarization and the contribution from the S atom is more than that of the Ti atom. As given in Table I, TiS_3 monolayer with a Ti-vacancy exhibits a magnetic ground state and the calculated magnetic moment is $0.5 \mu_B/\text{supercell}$.

C. Double S-vacancy

Possible two-atom-vacancy structures of TiS_3 are also investigated. First, the structure of double S atoms removed from the surface of TiS_3 is studied. Fig. 3(c) presents its fully relaxed configuration. Compared to the one S vacancy situation, the lattice is more deformed. The double vacancy of surface S atoms leads to a reconstruction of the bonds between the S atoms of neighboring prisms (dark green one) and the Ti atoms closest to the vacancies. These Ti atoms become more strongly bonded to the surface S atoms. However, compared to the defect-free structure, when two S atoms are removed the lattice parameters are slightly changed. Bader charge analysis shows that, removing two surface S atoms does not affect the charges of the remaining Ti atoms. However, 0.7 excess electrons of the removed two S atoms are shared by neighbor S atoms. The formation energy of double S-vacancy is 8.48 eV. Thus, removing two S atoms from the TiS_3 surface is more probable than removing one Ti atom.

The calculated density of states of monolayer TiS_3 with double S-vacancy is presented in Fig. 4(d). When the second S atom is taken out from the surface, TiS_3 exhibits metallic character. As seen from Fig. 4(d) the main contribution comes from the Ti atoms and TiS_3 with double S-vacancy has an asymmetric DOS at the Fermi level. This asymmetric DOS at the Fermi level leads to a magnetic ground state with the magnetic moment value of $0.8 \mu_B/\text{supercell}$.

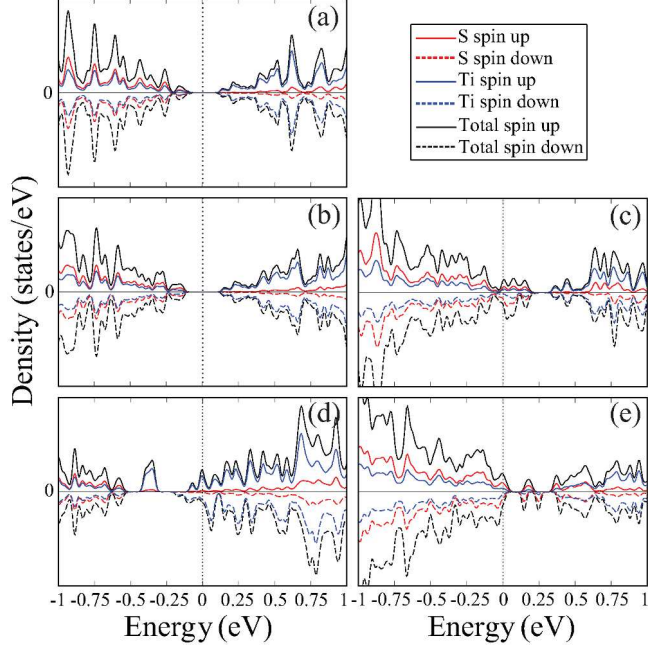


FIG. 4: Density of states of (a) pristine TiS_3 , with (b) S-vacancy, (c) Ti-vacancy, (d) Double S-vacancy, and (e) TiS-vacancy.

D. TiS-vacancy

Lastly, we considered the defected structure of TiS_3 with a TiS-vacancy. Fig. 3(d) shows that in the presence of TiS-vacancy, the position of the closest surface S atom to the removed S atom is significantly changed. This atom follows the direction of the arrow and becomes located at the top of the inner S atom (light green) with charge 6.6 electrons. Other two surface S atoms move toward the vacancies and their charges reduce to 6.0 and 6.2 electrons. The lattice parameters reduce to the values $a_1 = 14.90 \text{ \AA}$ and $a_2 = 10.13 \text{ \AA}$. Compared to the other vacancy types its formation energy value is the highest with the value 16.15 eV.

DOS diagram of TiS_3 with TiS-vacancy is illustrated in Fig. 4(e). Like Ti and double S-vacancies, this vacancy type also leads to a metallic character. But, unlike the double S-vacancy, Fermi level consists of orbitals of S atom. As given in Table I, the magnetic moment of this case is $0.3 \mu_B/\text{supercell}$.

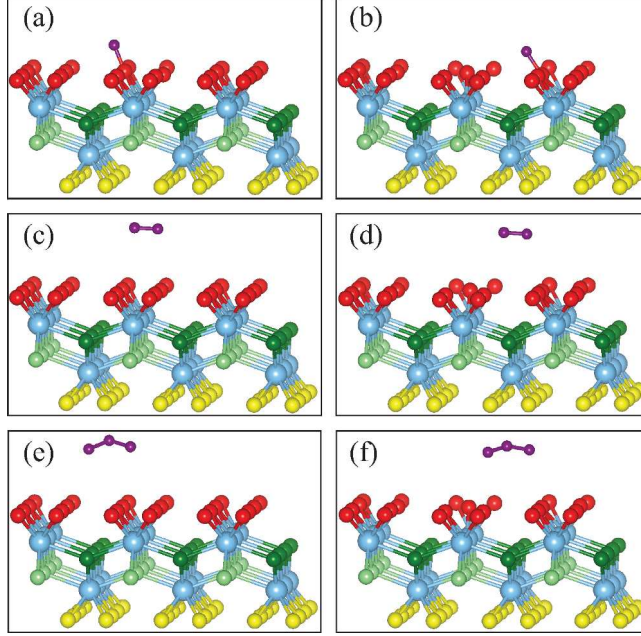


FIG. 5: (Color online) Tilted side view of (a) O, (c) O₂ and (e) O₃ adsorbed on pristine TiS₃. (b) O, (d) O₂ and (f) O₃ adsorbed on an S-vacant TiS₃.

V. OXIDATION OF PRISTINE AND DEFECTIVE TiS₃

It is well-known that two-dimensional ultra-thin structures such as graphene, MoS₂, phosphorene etc. are prone to oxidation.^{41–43} Therefore, the search for structural and environmental stability of TiS₃ is of importance. After the investigation of possible defect types in monolayer TiS₃, in this section we address the oxidation process and the role of vacancies in that process.

A. O atom adsorption on pristine and defective TiS₃

During experiments in highly oxidative conditions, the presence of Oxygen atom is inevitable and atomic O can be considered as a powerful tool to functionalize the surface of TiS₃. Thus, we start to investigate the oxidation with atomic O on pristine TiS₃. As shown in Fig. 5(a), the optimized structures show that, an O atom is adsorbed by an S atom on the pristine TiS₃ surface. The distance between O and S atoms is about 1.49 Å. The presence of the O atom does not have any significant effect on the lattice structure of TiS₃. O atom binds strongly to the S atom whose bond has an ionic character. The amount of

charge transfer between O and S atoms is about 1.3 electrons from S to the O atom. The binding energy of the O atom on TiS₃ crystal is -3.89 eV. When O atom binds to the TiS₃ surface, it loses its magnetic moment and the whole system does not exhibit any net magnetic moment.

The vacancy calculations have shown that the most probable defect type of TiS₃ is the S atom vacancy. Since the O atom readily binds to the pristine TiS₃ surface, the effect of the S-vacancy on the adsorption of atomic O is in order. Fig. 5(b) shows that, instead of being the nearest S atom to the vacancy, O atom prefers to bind to the other surface-S atom from tilted-top site. Compared to the pristine case, the presence of the S vacancy increases the binding energy of O atom from -3.89 eV to -4.01 eV. The bond distance between O and S atoms is 1.48 Å. Unlike the pristine case, O atom distorts the lattice of defective TiS₃ and the new lattice vectors are expanded to $a_1 = 14.93$ Å and $a_2 = 10.19$ Å. O atom binds ionically to the surface S atom and 1.1 electrons transfer from surface S atom to the O atom. Like in the pristine case, the net magnetic moment of the whole system is zero.

We also investigate substitutional adsorption of O atom on the surface of single layer TiS₃. The formation energy of the substitutional O atom at S site is calculated using the formula $E_{Subs} = E_{M+O} - E_M - E_O + E_S$, where E_{M+O} denotes the energy of O-doped TiS₃, E_M is the energy of pristine TiS₃, E_O and E_S are single atom energies. Substitution energy of O with S is found to be -1.38 eV. Negative value for O atom indicates the spontaneous formation of substitutional doping at the S site for O atom. It is also seen that the presence of substitutional O does not change the nonmagnetic structure of TiS₃.

B. O₂ molecule adsorption on pristine and defective TiS₃

Approximately 21% of the earth atmosphere is composed of O₂ molecules. Thus, the binding mechanism of O₂ molecule on TiS₃ surface and the stability of TiS₃ in the presence of this molecule are very crucial. The results of our calculations show that compared to atomic O, the O₂ molecule binds very weakly to the TiS₃ surface and its binding energy is -0.07 eV. Fig. 5(c) shows that O₂ locates 3.2 Å above the TiS₃ surface and it prefers to bind on top of the vicinity of S atom. The presence of O₂ on the TiS₃ surface does not cause any distortion on the lattice structure. Contrary to the single O atom case, there is no significant charge transfer between the surface and the molecule. Total magnetic moment

of the system is $2\mu_B$, which is equal to the magnetic moment of an isolated O_2 molecule.

The presence of an S-vacancy does not have any significant effect on the adsorption of O_2 molecule on the TiS_3 crystal. Similar to the pristine case, O_2 molecule binds rather weakly to S-vacancy with a binding energy of -0.05 eV. Compared to the pristine case, O_2 molecule is localized more close to the TiS_3 surface at a z-distance of 2.89 Å. The presence of O_2 molecule does not cause any notable distortion of the defected TiS_3 crystal. Like in the pristine case, there is almost no charge transfer between TiS_3 and the O_2 molecule and the net magnetic moment of O_2 molecule which is $2\mu_B$, does not change in the presence of the S-vacancy.

C. O_3 molecule adsorption on pristine and defective TiS_3

To complete the analysis of oxidation of TiS_3 , the binding mechanism of the O_3 molecule on the TiS_3 surface is investigated. It is found that, compared to O_2 molecule, O_3 molecule binds more strongly to the TiS_3 surface. Binding energy of O_3 molecule on TiS_3 surface is -0.21 eV. As seen from Fig. 5(e), O_3 molecule locates 3.15 Å above the TiS_3 surface with two edge O atoms being closer to the surface compared to the middle O atom. The stability of TiS_3 is not affected by O_3 . When the O_3 molecule is placed on the TiS_3 surface, it receives an extra 0.2 electrons from the TiS_3 . The net magnetic moment of the O_3 molecule adsorbed on pristine TiS_3 is zero.

Finally, the adsorption of O_3 molecule on an S-vacancy is investigated. As seen from Fig. 5(f), O_3 molecule locates approximately 2.95 Å above the TiS_3 surface. In the S vacancy case the end O atoms are placed closer to the surface compared to the middle O atom. Presence of S vacancy slightly affects the binding energy of O_3 molecule which is equal to -0.20 eV. O_3 molecule does not make any significant effect on the lattice structure of TiS_3 with an S-vacancy. The charge transfer from the surface to the molecule is about 0.2 electrons. The adsorbed O_3 molecule on an S-vacancy does not possess any net magnetic moment.

VI. CONCLUSION

In this paper, a detailed analyses of structural, electronic and magnetic properties of pristine, defective and oxidized structures of monolayer TiS_3 are presented by using first-

principles calculations. In addition to the PBE version of GGA, the HSE06 form of hybrid functionals were also used to describe the exchange-correlation density functional. Electronic structure calculations using HSE06 hybrid functional indicated that monolayer TiS_3 is a direct bandgap semiconductor with a band gap of 1.05 eV. Our calculations also revealed interesting bonding nature of the monolayer TiS_3 crystal that has ionic character inside and covalent character for surface atoms. The negatively charged surface of the crystal may also find some interesting applications such as nanoscale lubricants and charged coatings.

Among various vacancy defects including S, Ti, TiS and double S vacancies, the single S vacancy has the lowest formation energy. While the S vacancy leads to an opening in the band gap, other vacancies result in metallicity in single layer TiS_3 . Pristine and S vacancy defected TiS_3 does not possess any net magnetic moment, whereas other considered vacancies are magnetic. Our DFT oxidation studies revealed that, TiS_3 readily oxidizes with atomic O. Moreover, it is found that, oxidation of TiS_3 with O_3 is most likely to occur, while oxidation with O_2 is less favorable on pristine and S defected TiS_3 surface. S vacancy has a slightly negative effect on the adsorption of O_2 and O_3 molecules on TiS_3 surface, however it has a favoring effect on the adsorption of atomic O.

Acknowledgments

This work was supported by the Flemish Science Foundation (FWO-VI) and the Methusalem foundation of the Flemish government. Computational resources were provided by TUBITAK ULAKBIM, High Performance and Grid Computing Center (TR-Grid e-Infrastructure), and HPC infrastructure of the University of Antwerp (CalcUA) a division of the Flemish Supercomputer Center (VSC), which is funded by the Hercules foundation. H.S. is supported by a FWO Pegasus Marie Curie Fellowship. F.I., H.S. and R.T.S. acknowledge the support from TUBITAK through project 114F397.

* Electronic address: fadiliyikanat@iyte.edu.tr

† Electronic address: hasan.sahin@uantwerpen.be

¹ Novoselov, K. S.; Geim, A. K.; Morozov, S. V.; Jiang, D.; Zhang, Y.; Dubonos, S. V.; Grigorieva, I. V.; Firsov, A. A. Electric Field Effect in Atomically Thin Carbon Films. *Science* **2004**, *306*

- (5696), 666-669.
- ² Geim, A. K.; Novoselov, K. S. The Rise of Graphene. *Nat. Mater.* **2007**, *6* (3), 183-191.
 - ³ Wang, Q. H.; Zadeh, K. K.; Kis, A.; Coleman, J. N.; Strano, M. S. Electronics and Optoelectronics of Two-Dimensional Transition Metal Dichalcogenides. *Nat. Nanotechnol.* **2012**, *7* (11), 699-712.
 - ⁴ Xu, M.; Liang, T.; Shi, M.; Chen, H. Graphene-Like Two-Dimensional Materials. *Chem. Rev.* **2013**, *113* (5), 3766-3798.
 - ⁵ Huang, X.; Zeng, Z.; Zhang, H. Metal Dichalcogenide Nanosheets: Preparation, Properties and Applications. *Chem. Soc. Rev.* **2013**, *42* (5), 1934-1946.
 - ⁶ Wilson J. A.; Yoffe, A. D. The Transition Metal Dichalcogenides Discussion and Interpretation of the Observed Optical, Electrical and Structural Properties. *Adv. Phys.* **1969**, *18* (73), 193-335.
 - ⁷ Zhang, Q.; Li, G.; Rhodes, D.; Kiswandhi, A.; Besara, T.; Zeng, B.; Sun, J.; Siegrist, T.; Johannes, M. D.; Balicas, L. Superconductivity with Extremely Large Upper Critical Fields in Nb₂Pd_{0.81}S₅. *Sci. Rep.* **2013**, *3*.
 - ⁸ Ang, R.; Miyata, Y.; Ieki, E.; Nakayama, K.; Sato, T.; Liu, Y.; Lu, W. J.; Sun, Y. P.; Takahashi, T. Superconductivity and Bandwidth-Controlled Mott Metal-Insulator Transition in 1T-TaS_{2-x}Se_x. *Phys. Rev. B* **2013**, *88* (11), 115145.
 - ⁹ Splendiani, A.; Sun, L.; Zhang, Y.; Li, T.; Kim, J.; Chim, C.-Y.; Galli, G.; Wang, F. Emerging Photoluminescence in Monolayer MoS₂. *Nano Lett.* **2010**, *10* (4), 1271-1275.
 - ¹⁰ Ataca, C.; Sahin, H.; Ciraci, S. Stable, Single-Layer MX₂ Transition-Metal Oxides and Dichalcogenides in a Honeycomb-Like Structure. *J. Phys. Chem. C* **2012**, *116* (16), 8983-8999.
 - ¹¹ Di Salvo, F. J.; Moncton, D. E.; Waszczak, J. V. Electronic Properties and Superlattice Formation in the Semimetal TiSe₂. *Phys. Rev. B* **1976**, *14* (10), 4321.
 - ¹² Wang, H.; Yu, L.; Lee, Y.-H.; Shi, Y.; Hsu, A.; Chin, M. L.; Li, L.-J.; Dubey, M.; Kong, J.; Palacios, T. Integrated Circuits Based on Bilayer MoS₂ Transistors. *Nano Lett.* **2012**, *12* (9), 4674-4680.
 - ¹³ Nicolosi, V.; Chhowalla, M.; Kanatzidis, M. G.; Strano, M. S.; Coleman, J. N. Liquid Exfoliation of Layered Materials. *Science* **2013**, *340* (6139), 1226419.
 - ¹⁴ Chhowalla, M.; Shin, H. S.; Eda, G.; Li, L.-J.; Loh, K. P.; Zhang, H. The Chemistry of Two-Dimensional Layered Transition Metal Dichalcogenide Nanosheets. *Nat. Chem.* **2013**, *5* (4),

- 263-275.
- ¹⁵ Iyikanat, F.; Sahin, H.; Senger, R. T.; Peeters, F. M. Ag and Au Atoms Intercalated in Bilayer Heterostructures of Transition Metal Dichalcogenides and Graphene. *APL Mat.* **2014**, *2* (9), 092801.
 - ¹⁶ Mak, K. F.; Lee, C.; Hone, J.; Shan, J.; Heinz, T. F. Atomically Thin MoS₂: A New Direct-Gap Semiconductor. *Phys. Rev. Lett.* **2010**, *105* (13), 136805.
 - ¹⁷ Horzum, S.; Cakir, D.; Suh, J.; Tongay, S.; Huang, Y.-S.; Ho, C.-H.; Wu, J.; Sahin, H.; Peeters, F. M. Formation and Stability of Point Defects in Monolayer Rhenium Disulfide. *Phys. Rev. B* **2014**, *89* (15), 155433.
 - ¹⁸ Zeng, H.; Dai, J.; Yao, W.; Xiao, D.; Cui, X. Valley Polarization in MoS₂ Monolayers by Optical Pumping. *Nat. Nanotech.* **2012**, *7* (8), 490-493.
 - ¹⁹ Brattas, L.; Kjekshus, A. On the Properties of Compounds with the ZrSe₃ Type Structure. *Acta Chem. Scand.* **1972**, *26* (9), 3441-3449.
 - ²⁰ Furuseth, S.; Brattas, L.; Kjekshus, A. On the Crystal Structures of TiS₃, ZrS₃, ZrSe₃, ZrTe₃, HfS₃, and HfSe₃. *Acta Chem. Scand. A* **1975**, *29*, 623-631.
 - ²¹ Finkman E.; Fisher, B. Electrical Transport Measurements in TiS₃. *Solid State Comm.* **1984**, *50* (1), 25-28.
 - ²² Gorlova, I. G.; Zybtshev, S. G.; Pokrovskii, V. Y.; Bolotina, N. B.; Verin, I. A.; Titov, A. N. Nonlinear Conductivity of Quasi-One-Dimensional Layered Compound TiS₃. *Physica B* **2012**, *407* (11), 1707-1710.
 - ²³ Gorlova, I. G.; Pokrovskii, V. Y.; Zybtshev, S. G.; Titov, A. N.; Timofeev, V. N. Features of the Conductivity of the Quasi-One-Dimensional Compound TiS₃. *J. Exp. Theo. Phys.* **2010**, *111* (2), 298-303.
 - ²⁴ Ferrer, I. J.; Ares, J. R.; Clamagirand, J. M.; Barawi, M.; Sanchez, C. Optical properties of titanium trisulphide (TiS₃) thin films. *Thin Solid Films* **2012**, *535*, 398-401.
 - ²⁵ Ferrer, I. J.; Marciá, M. D.; Carcelén, V.; Ares, J. R.; Sánchez, C. On the Photoelectrochemical Properties of TiS₃ Films. *Energy Procedia* **2012**, *22*, 48-52.
 - ²⁶ Guilmeau, E.; Berthebaud, D.; Misse, P. R. N.; Hébert, S.; Lebedev, O. I.; Chateigner, D.; Martin, C.; Maignan, A. ZrSe₃-Type Variant of TiS₃: Structure and Thermoelectric Properties. *Chem. Mater.* **2014**, *26* (19), 5585-5591.
 - ²⁷ Island, J. O.; Buscema, M.; Barawi, M.; Clamagirand, J. M.; Ares, J. R.; Sánchez, C.; Ferrer,

- I. J.; Steele, G. A.; van der Zant, H. S. J.; Gomez, A. C. Ultrahigh Photoresponse of Few-Layer TiS₃ Nanoribbon Transistors. *Adv. Opt. Mater.* **2014**, *2* (7), 641-645.
- ²⁸ Island, J. O.; Barawi, M.; Biele, R.; Almazan, A.; Clamagirand, J. M.; Ares, J. R.; Sanchez, C.; van der Zant, H. S. J.; Alvarez, J. V.; D'Agosta, R.; et al. TiS₃ Transistors with Tailored Morphology and Electrical Properties. *Adv. Mater.* **2015**, *27* (16), 2595-2601.
- ²⁹ Barawi, M.; Flores, E.; Ferrer, I. J.; Ares, J. R.; Sanchez, C. Titanium Trisulphide (TiS₃) Nanoribbons for Easy Hydrogen Photogeneration Under Visible Light. *J. Mater. Chem. A* **2015**, *3* (15), 7959-7965.
- ³⁰ Gorlava, I. G.; Zybtssev, S. G.; Pokrovskii, V. Ya. Conductance Anisotropy and the Power-Law Current-Voltage Characteristics Along and Across the Layers of the TiS₃ Quasi-One-Dimensional Layered Semiconductor. *JETP Lett.* **2014**, *100* (4), 256-261.
- ³¹ Gorlava, I. G.; Zybtssev, S. G.; Pokrovskii, V. Ya.; Bolotina, N. B.; Gavrilkin, S. Yu.; Tsvetkov, A. Yu. Magnetotransport and Power-Law IV Curves of the Layered Quasi One-Dimensional Compound TiS₃. *Physica B* **2015**, *460*, 11-15.
- ³² Tanibata, N.; Matsuyama, T.; Hayashi, A.; Tatsumisago, M. All-Solid-State Sodium Batteries Using Amorphous TiS₃ Electrode with High Capacity. *J. Power Sources* **2015**, *275*, 284-287.
- ³³ Wu, J.; Wang, D.; Liu, H.; Lau, W.-M.; Liu, L.-M. An Ab Initio Study of TiS₃: a Promising Electrode Material for Rechargeable Li and Na Ion Batteries. *RSC Adv.* **2015**, *5* (28), 21455-21463.
- ³⁴ Jin, Y.; Li, X.; Yang, J. Single Layer of MX₃ (M=Ti, Zr; X=S, Se, Te): a New Platform for Nano-Electronics and Optics. 2015, arXiv:1502.05108 [cond-mat.mtrl-sci]. arXiv.org e-Print archive. <http://arxiv.org/abs/1502.05108> (accessed Feb 18, 2015)
- ³⁵ Kresse G.; Furthmüller, J. Efficient Iterative Schemes for Ab Initio Total-Energy Calculations Using a Plane-Wave Basis Set. *Phys. Rev. B* **1996**, *54* (16), 11169.
- ³⁶ Kresse, G.; Joubert, D. From ultrasoft pseudopotentials to the projector augmented-wave method. *Phys. Rev. B* **1999**, *59* (3), 1758.
- ³⁷ Perdew, J. P.; Burke, K.; Ernzerhof, M. Generalized Gradient Approximation Made Simple. *Phys. Rev. Lett.* **1996**, *77* (18), 3865.
- ³⁸ Heyd, J.; Scuseria, G. E.; Ernzerhof, M. Erratum: "Hybrid functionals based on a screened Coulomb potential." *J. Chem. Phys.* **2006**, *124* (21), 219906.
- ³⁹ Henkelman, G.; Arnaldsson, A.; Jonsson, H. A fast and robust algorithm for Bader decom-

- position of Charge Density. *Comp. Mat. Sci.* **2006**, *36* (3), 354-360.
- ⁴⁰ Grimme, S. Semiempirical GGA-Type Density Functional Constructed with a Long-Range Dispersion Correction. *J. Comp. Chem.* **2006**, *27* (15), 1787-1799.
- ⁴¹ Vinogradov, N. A.; Schulte, K.; Ng, M. L.; Mikkelsen, A.; Lundgreen, E.; Martensson, N.; Preobrajenski, A. B. Impact of Atomic Oxygen on the Structure of Graphene Formed on Ir(111) and Pt(111). *J. Phys. Chem. C* **2011**, *115* (19), 9568-9577.
- ⁴² Wang, G.; Pandey, R.; Karna, S. P. Effects of Extrinsic Point Defects in Phosphorene: B, C, N, O and F Adatoms. 2015, arXiv:1503.04165 [physics.chem-ph]. arXiv.org e-Print archive. <http://arxiv.org/abs/1503.04165> (accessed Mar 13, 2015)
- ⁴³ Yamamoto, M.; Einstein, T. L.; Fuhrer, M. S.; Cullen, W. G. Anisotropic Etching of Atomically Thin MoS₂. *J. Phys. Chem. C* **2013**, *117* (48), 25643-25649.

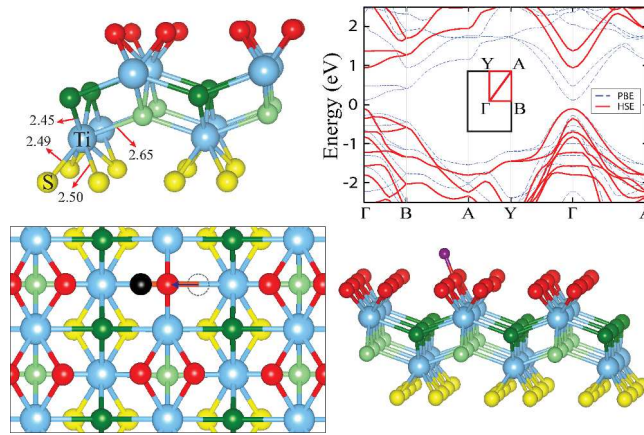


FIG. 6: For Table of Contents Only.